

Rethinking the Open-Loop Evaluation of End-to-End Autonomous Driving in nuScenes

Jiang-Tian Zhai* Ze Feng* Jinhao Du* Yongqiang Mao* Jiang-Jiang Liu†
 Zichang Tan Yifu Zhang Xiaoqing Ye Jingdong Wang†

Baidu Inc.

{jtzhai30, j04.liu}@gmail.com, wangjingdong@outlook.com

Abstract

Modern autonomous driving systems are typically divided into three main tasks: perception, prediction, and planning. The planning task involves predicting the trajectory of the ego vehicle based on inputs from both internal intention and the external environment, and manipulating the vehicle accordingly. Most existing works evaluate their performance on the nuScenes dataset using the L2 error and collision rate between the predicted trajectories and the ground truth. In this paper, we reevaluate these existing evaluation metrics and explore whether they accurately measure the superiority of different methods. Specifically, we design an MLP-based method that takes raw sensor data (e.g., past trajectory, velocity, etc.) as input and directly outputs the future trajectory of the ego vehicle, without using any perception or prediction information such as camera images or LiDAR. Our simple method achieves similar end-to-end planning performance on the nuScenes dataset with other perception-based methods, reducing the average L2 error by about 20%. Meanwhile, the perception-based methods have an advantage in terms of collision rate. We further conduct in-depth analysis and provide new insights into the factors that are critical for the success of the planning task on nuScenes dataset. Our observation also indicates that we need to rethink the current open-loop evaluation scheme of end-to-end autonomous driving in nuScenes. Codes are available at <https://github.com/E2E-AD/AD-MLP>.

1. Introduction

Many existing autonomous driving models [12, 15, 16] involve a multi-stage pipeline of independent tasks, such as perception [11, 17], prediction [4, 5] and planning [2, 3].

*Equal contribution.

†Project lead.

While this design simplifies the difficulty of collaboration across teams, it leads to information loss and error accumulation in the overall system due to the independence of optimization targets and model training. To better predict control signals and enhance user safety, an end-to-end approach that benefits from spatial-temporal feature learning from the ego vehicle and surrounding environment is desired.

Planning for autonomous driving is the ultimate goal of the entire system. To achieve these, some methods are accomplished through perception tasks, such as 3D object detection and semantic segmentation to obtain temporal and spatial information about the surrounding environment. A natural idea is that if a model can perform well in these perception tasks, it can make accurate, safe, and comfortable trajectory planning based on this information. ST-P3 [7] proposes an interpretable vision-based end-to-end system that unifies feature learning for perception, prediction, and planning. UniAD [8] adopts a systematic model design for the planning task by connecting all intermediate task nodes based on the query-based design where the relationship between multiple tasks can be modeled and encoded. VAD [9] models the scene in a fully vectorized way, getting rid of computationally intensive grid feature representation and being more efficient in computation. This vectorized feature representation helps autonomous driving vehicles focus on the crucial map and agent elements, and plan a reasonable future trajectory. The above-mentioned methods achieve promising performance on the trajectory planning task of the ego vehicle on the nuScenes [1] dataset, which is the most commonly used one in the area.

However, in this paper, in order to explore whether the existing evaluation metrics can accurately measure the superiority of different methods, we only use the physical state of the ego vehicle during driving as input (*i.e.*, a subset of the information used by existing methods) to conduct experiments, instead of using the perception and prediction information provided by the camera or LiDAR. In other

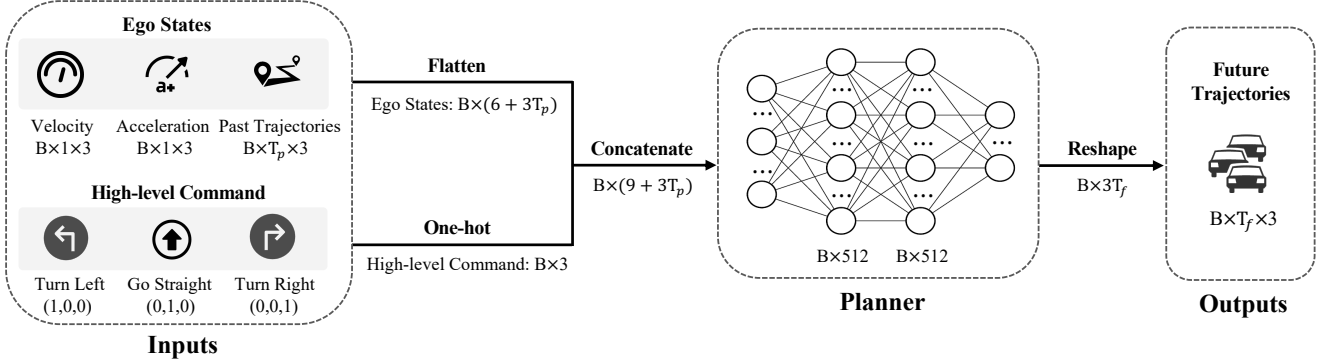


Figure 1. Overall pipeline. **Inputs:** 1) ego vehicle’s states: motion trajectories (x, y, θ) of the past T_p frames (in our experiments $T_p = 4$), instantaneous velocity (v_x, v_y, ω) and acceleration (a_x, a_y, β) . θ, ω , and β indicate heading angle, angular velocity, and angular acceleration, respectively; 2) high-level command (one-hot encoded). B indicates batch size. **Outputs:** motion trajectory of the ego vehicle in the future T_f frames (in our experiments $T_f = 6$).

words, there is no encoder for visual or point cloud feature extraction in the model. We directly unfold all the physical information of the ego vehicle into one-dimensional vectors and feed them into a multi-layer perceptron (MLP) after concatenation.

During training, we use the ground-truth trajectory as supervision and have the model directly predict the ego vehicle’s future trajectory points for a certain period of time. Following previous methods [7, 8], we validate our approach on the nuScenes dataset using the metrics of L2 error and collision rate.

Although the design of our model is simple and no perception information is utilized, it achieves similar trajectory planning performance on the nuScenes dataset. We attribute this to the inadequacy of current evaluation metrics for planning tasks on the nuScenes dataset to accurately compare the performance of different methods. In fact, the motion of the ego vehicle in the future can be reflected to a certain extent by using the past trajectory, velocity, acceleration information, and temporal continuity.

2. Method

The overall pipeline of our method is illustrated in Figure 1. As our model requires no perception information, there is no component for visual or point-cloud feature extraction. The inputs only consist of two parts: the ego states and the high-level command representing its future short-term motion trend. Our model is trained in an end-to-end manner.

2.1. Model Inputs

Ego States. Following [9], we collect the ego vehicle’s motion trajectories of the past $T_p = 4$ frames, instantaneous velocity and acceleration as input. The trajectory of each frame consists of three values: (x, y, θ) , repre-

senting the position and heading angle of ego vehicle, respectively. The instantaneous velocity (v_x, v_y, ω) and acceleration (a_x, a_y, β) represent the current x -directional, y -directional, and angular velocity and acceleration, respectively. We obtain this information from the nuScenes CAN bus expansion. The above-mentioned ego states are then flattened and concatenated into a one-dimensional vector.

High-Level Command. Since our model does not use HD maps as input, a high-level command is required for navigation. Following the common practice [7, 8], three types of commands are defined: turn left, go straight, and turn right. Specifically, when the ego vehicle displaces $> 2m$ to the left or right direction in the future 3s, the corresponding command is set to turn left or right. Otherwise, it corresponds to going straight. We represent the command using a 1×3 one-hot encoding.

The ego states and high-level command are concatenated together as the network’s inputs, so the final dimension of the input vector is 21.

Network Structure. The structure of our model is a simple MLP and can be summarized as $Linear^{21}_{512} - ReLU - Linear^{512}_{512} - ReLU - Linear^{512}_{18}$. For each $Linear^{C_{out}}_{C_{in}}$, C_{in} and C_{out} represent the numbers of input and output channels, respectively. The final outputs represent the ego vehicle’s trajectories (x, y coordinates) and heading angles for the future $T_f = 6$ frames.

2.2. Loss Function

The loss function \mathcal{L} is implemented with a L1 loss between the predicted planning trajectories \hat{V}_{ego} and the ground-truth ego trajectories V_{ego} , which can be formulated as follows:

$$\mathcal{L} = \frac{1}{N_f} \sum_{i=1}^{N_f} \|\hat{V}_{ego} - V_{ego}\|_1 \quad (1)$$

Method	Perception Information	High-level Command	Ego State			L2 (m) ↓				Collision (%) ↓			
			Velocity	Acceleration	Trajectory	1s	2s	3s	Avg.	1s	2s	3s	Avg.
NMP [18]	✓	✗	-	-	-	-	-	2.31	-	-	-	1.92	-
SA-NMP [18]	✓	✗	-	-	-	-	-	2.05	-	-	-	1.59	-
FF [6]	✓	✗	-	-	-	0.55	1.20	2.54	1.43	0.06	0.17	1.07	0.43
EO [10]	✓	✗	-	-	-	0.67	1.36	2.78	1.60	0.04	0.09	0.88	0.33
ST-P3 [7]	✓	✓	-	-	-	1.33	2.11	2.90	2.11	0.23	0.62	1.27	0.71
UniAD [8]	✓	✓	-	-	-	0.48	0.96	1.65	1.03	0.05	0.17	0.71	0.31
VAD-Tiny [9]	✓	✓	✓	✓	✓	0.20	0.38	0.65	0.41	0.10	0.12	0.27	0.16
VAD-Base [9]	✓	✓	✓	✓	✓	0.17	0.34	0.60	0.37	0.07	0.10	0.24	0.14
Ours	✗	✗	-	-	✓	0.53	0.91	1.48	0.97	0.17	0.46	0.83	0.49
	✗	✗	-	✓	✓	0.33	0.48	0.66	0.49	0.21	0.29	0.40	0.30
	✗	✗	✓	✓	✓	0.24	0.32	0.49	0.35	0.18	0.22	0.28	0.23
	✗	✓	✓	✓	✓	0.20	0.26	0.41	0.29	0.17	0.18	0.24	0.19

Table 1. Comparison with existing perception-based methods. Our method achieves slightly lower L2 error, while the collision rate is higher than some other methods. Results in the table except for our method are collected from VAD [9].

where N_f denotes the number of future frames, *e.g.*, 6. Since the resolution of occupancy map is 0.5m for one grid, the predicted trajectory point is mapped to the same grid if it falls into the same 0.5m segment, *e.g.*, [1.5m, 2m), with the ground truth on both x and y axes. We re-weight the loss by 0.5 on samples where the predicted trajectory points and the ground truth coincide at the same grid for hard sample mining to reduce the collision rate.

3. Experiments

3.1. Dataset & Evaluation Metrics

Dataset. Following the common practice [7–9] in the planning task, we use the nuScenes [1] dataset in our experiments for both training and testing. The dataset includes 1K scenes and approximately 40K key-frames mainly collected in Boston and Singapore using vehicles equipped with both LiDAR and surrounding cameras. The data collected for each frame includes multi-view camera images, LiDAR, velocity, acceleration, etc.

Metrics. We use the implementation¹ provided by ST-P3 [7] to evaluate the output trajectories for time horizons of 1s, 2s, and 3s. To evaluate the quality of the predicted ego trajectories, two commonly used metrics [7–9] are calculated: L2 error (in meters) and collision rate (in percentage). The average L2 errors are calculated between the predicted and ground-truth trajectories for corresponding waypoints within the next 1s, 2s, and 3s time horizons, respectively. To determine how often the ego vehicle collides with other objects, the collision rate is computed by placing a box rep-

resenting the ego vehicle at each waypoint on the predicted trajectory and then detecting if any collision with other oriented bounding boxes that represent vehicles and pedestrians in the scene occurs.

3.2. Implementation Details

Our model is implemented in both the PaddlePaddle and PyTorch framework. The AdamW [14] optimizer is used with an initial learning rate of 4e-6 and weight decay of 1e-2. The cosine annealing [13] learning rate schedule is utilized. Our model is trained for 6 epochs with a batch size of 4 on 1 NVIDIA Tesla V100 GPUs.

3.3. Main Results

We conduct some ablation experiments in Table 1 to analyze the impact of velocity, acceleration, trajectories, and high-level command information to the performance of our model. We gradually add the acceleration, velocity, and high-level command information to the input, the average L2 error and collision rate continually decrease from 0.97m to 0.29m, and 0.49% to 0.19%. It is worth mentioning that the collision rate of our method is not as low as some perception-based methods. We believe this is due to the insufficient decision-making process resulting from the mere fitting of motion information, which raises safety concerns. Besides, the difference of average collision rates between our method and the others (*e.g.*, 0.19% v.s. 0.14%) represents only about 2 ~ 3 samples in all 4819 ones. We believe that more discriminative testing scenarios are needed to better demonstrate the advantages of perception-based methods.

¹<https://github.com/OpenPerceptionX/ST-P3/blob/main/stp3/metrics.py>

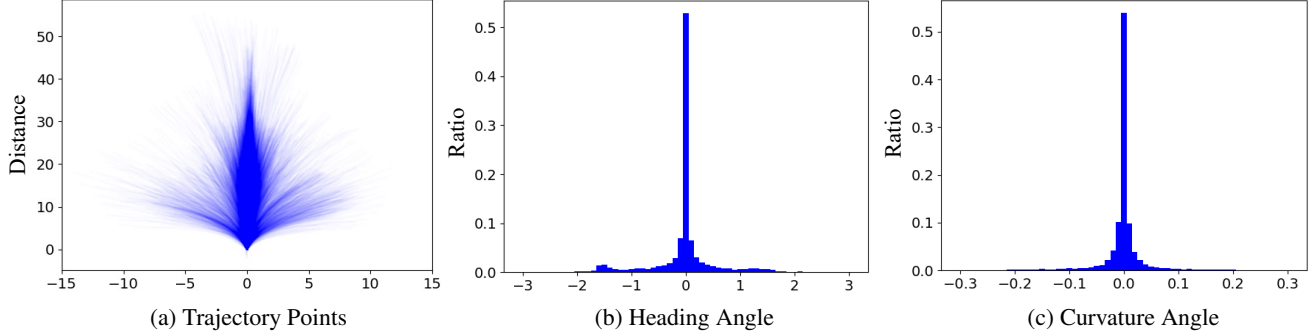


Figure 2. Distribution analysis of nuScenes training set. The trajectory points are concentrated in the middle forward area, and the heading angle and curvature angle are concentrated around radian 0. We can conclude that most cases of the ego vehicle are in straight and small angles forward, and there are few cases of large angle turns.

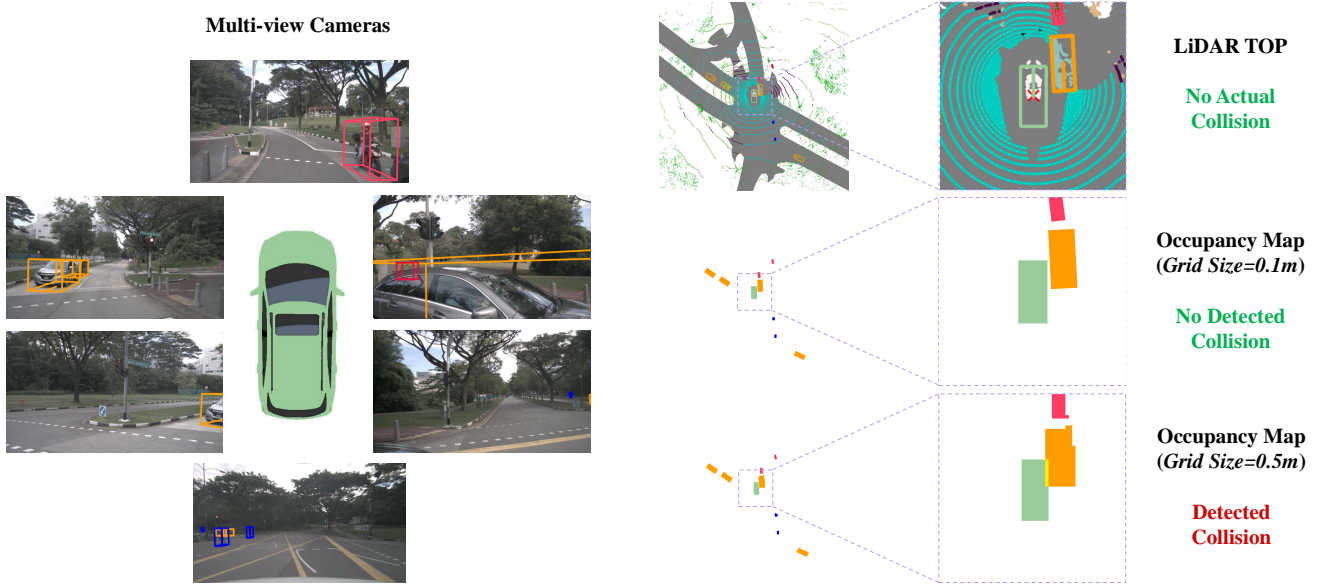


Figure 3. A typical ground-truth trajectory collision case caused by different grid sizes of the occupancy maps. It can be observed that the grid size for occupancy map generating has a great impact on the collision test, which is commonly used in the evaluation of collision in existing methods. For instance, in the case of $grid\ size = 0.1m$, the ground-truth trajectory is correctly recognized as a no-collision case while being misjudged when $grid\ size = 0.5m$. We can also find from the bottom-right of the figure that when $grid\ size = 0.5m$, some object masks even become irregular, which are supposed to be rectangles (e.g., the orange and red ones).

4. Analysis and Discussion

4.1. Trajectory Distribution of nuScenes

This sub-section mainly analyzes the distribution of the ego vehicle’s states on the nuScenes training set from two perspectives: trajectory points in the future 3s, heading and curvature angles.

Trajectory Points. We plot all future 3s trajectory points in the training set in Figure 2 (a). It can be seen from the figure that the trajectories are largely concentrated in the middle part (go straight), and the trajectories are mainly straight lines, or curves with very small curvatures.

Heading and Curvature Angles. The heading angle indicates the future driving direction relative to the current time, while the curvature angle reflects the vehicle’s turning rate. As illustrated in Figure 2 (b) and (c), nearly 70% of the heading angles and curvature angles lie within the ranges of -0.2 to 0.2 and -0.02 to 0.02 radians, respectively. This finding is consistent with the conclusion drawn from the distribution of trajectory points.

Based on the above analysis on the distributions of the trajectory points, heading and curvature angles, we argue that in the nuScenes training set, ego vehicles tend to move forward along straight lines and at small angles during driv-

ing in short-time horizons.

4.2. Collision in Ground Truth

When calculating the collision rate, the common practice of existing methods is to first project objects such as vehicles and pedestrians into the bird’s-eye-view (BEV) space and then convert them into occupied regions in the occupancy map, where loss of precision occurs. After this process, we find that a small fraction of ground-truth trajectory samples (about 2%) also overlap with obstacles in the occupancy grid, resulting in collisions being falsely detected.

However, the ego vehicle does not actually collide with any other objects while collecting data annotations. This anomaly is due to employing an occupancy map with a relatively large grid size, leading to false collisions when the ego vehicle approaches certain objects, *e.g.*, smaller than the size of a single occupancy map pixel. We show an example of this phenomenon in Figure 3, together with the collision detection results of ground-truth trajectories for two different grid sizes. Under a smaller grid size (0.1m) shown in the middle-right, the evaluation system correctly identifies the ground-truth trajectory as not colliding, but under a larger grid size (0.5m) in the bottom-right, a false collision detection occurs.

After observing the impact of occupancy grid size on trajectory collision detection, we test with a grid size of 0.6m. The nuScenes training set has 4.8% collision samples, while the validation set has 3.0%. It is worth mentioning that when we previously use a grid size of 0.5m, only 2.0% of the samples in the validation set are misclassified as collisions. This proves once again that the current method for determining the collision rate is not robust and accurate enough.

5. Conclusion and Limitations

In this paper, we rethink the conventional evaluation metrics used in end-to-end autonomous driving by employing a simple MLP-based model that solely relies on physical states without any visual or point cloud perception as input. Despite its simplicity and the absence of perceptual information, our model achieves similar performance on the nuScenes dataset, suggesting that the current evaluation metrics may not adequately capture the superiority of different methods.

Limitations. The primary objective of this paper is to present our observations rather than propose a new model. Our findings demonstrate the potential limitations of the current evaluation scheme on the nuScenes dataset. Although our model performs well within the confines of the nuScenes dataset, we acknowledge that it is merely an impractical toy incapable of functioning in real-world scenarios. Driving without any knowledge beyond the ego vehicle’s states is an insurmountable challenge.

We believe that perception-based planning methods will ultimately become the solution to autonomous driving, producing much safer trajectories than our toy model. We hope that our insights will stimulate further research in the field, encouraging a reevaluation and enhancement of the planning task for end-to-end autonomous driving.

References

- [1] Holger Caesar, Varun Bankiti, Alex H Lang, Sourabh Vora, Venice Erin Liang, Qiang Xu, Anush Krishnan, Yu Pan, Giacomo Baldan, and Oscar Beijbom. nuScenes: A multi-modal dataset for autonomous driving. In *CVPR*, 2020. [1](#), [3](#)
- [2] Long Chen, Lukas Platinsky, Stefanie Speichert, Blazej Osinski, Oliver Scheel, Yawei Ye, Hugo Grimmett, Luca Del Pero, and Peter Ondruska. What data do we need for training an AV motion planner? In *ICRA*, 2021. [1](#)
- [3] Kashyap Chitta, Aditya Prakash, Bernhard Jaeger, Zehao Yu, Katrin Renz, and Andreas Geiger. Transfuser: Imitation with transformer-based sensor fusion for autonomous driving. *IEEE TPAMI*, 2022. [1](#)
- [4] Junru Gu, Chen Sun, and Hang Zhao. Densentnt: End-to-end trajectory prediction from dense goal sets. In *ICCV*, 2021. [1](#)
- [5] Anthony Hu, Zak Murez, Nikhil Mohan, Sofía Dudas, Jeffrey Hawke, Vijay Badrinarayanan, Roberto Cipolla, and Alex Kendall. FIERY: Future instance segmentation in bird’s-eye view from surround monocular cameras. In *ICCV*, 2021. [1](#)
- [6] Peiyun Hu, Aaron Huang, John Dolan, David Held, and Deva Ramanan. Safe local motion planning with self-supervised freespace forecasting. In *CVPR*, 2021. [3](#)
- [7] Shengchao Hu, Li Chen, Penghao Wu, Hongyang Li, Junchi Yan, and Dacheng Tao. St-p3: End-to-end vision-based autonomous driving via spatial-temporal feature learning. In *ECCV*, 2022. [1](#), [2](#), [3](#)
- [8] Yihan Hu, Jiazhi Yang, Li Chen, Keyu Li, Chonghao Sima, Xizhou Zhu, Siqi Chai, Senyao Du, Tianwei Lin, Wenhui Wang, Lewei Lu, Xiaosong Jia, Qiang Liu, Jifeng Dai, Yu Qiao, and Hongyang Li. Planning-oriented autonomous driving. In *CVPR*, 2023. [1](#), [2](#), [3](#)
- [9] Bo Jiang, Shaoyu Chen, Qing Xu, Bencheng Liao, Jiajie Chen, Helong Zhou, Qian Zhang, Wenyu Liu, Chang Huang, and Xinggang Wang. Vad: Vectorized scene representation for efficient autonomous driving. *arXiv preprint arXiv:2303.12077*, 2023. [1](#), [2](#), [3](#)
- [10] Tarasha Khurana, Peiyun Hu, Achal Dave, Jason Ziglar, David Held, and Deva Ramanan. Differentiable raycasting for self-supervised occupancy forecasting. In *ECCV*, 2022. [3](#)
- [11] Zhiqi Li, Wenhui Wang, Hongyang Li, Enze Xie, Chonghao Sima, Tong Lu, Yu Qiao, and Jifeng Dai. Bevformer: Learning bird’s-eye-view representation from multi-camera images via spatiotemporal transformers. In *ECCV*, 2022. [1](#)
- [12] Ming Liang, Bin Yang, Wenyuan Zeng, Yun Chen, Rui Hu, Sergio Casas, and Raquel Urtasun. Pnpnet: End-to-end per-

ception and prediction with tracking in the loop. In *CVPR*, 2020. 1

- [13] Ilya Loshchilov and Frank Hutter. Sgdr: Stochastic gradient descent with warm restarts. In *ICLR*, 2017. 3
- [14] Ilya Loshchilov and Frank Hutter. Decoupled weight decay regularization. In *ICLR*, 2019. 3
- [15] Wenjie Luo, Bin Yang, and Raquel Urtasun. Fast and furious: Real time end-to-end 3d detection, tracking and motion forecasting with a single convolutional net. In *CVPR*, 2018. 1
- [16] Abbas Sadat, Sergio Casas, Mengye Ren, Xinyu Wu, Pranaab Dhawan, and Raquel Urtasun. Perceive, predict, and plan: Safe motion planning through interpretable semantic representations. In *ECCV*, 2020. 1
- [17] Kaixin Xiong, Shi Gong, Xiaoqing Ye, Xiao Tan, Ji Wan, Errui Ding, Jingdong Wang, and Xiang Bai. Cape: Camera view position embedding for multi-view 3d object detection. In *CVPR*, 2023. 1
- [18] Wenyuan Zeng, Wenjie Luo, Simon Suo, Abbas Sadat, Bin Yang, Sergio Casas, and Raquel Urtasun. End-to-end interpretable neural motion planner. In *CVPR*, 2019. 3